

# Effect of TIG welding on Al Alloy, Mg Alloy, and Stainless Steel - A Review

Yogesh Dubey<sup>1\*</sup>, Pankaj Sharma<sup>2</sup> and Mahendra Pratap Singh<sup>3</sup>

<sup>1</sup>Department of Mechanical Engineering, JECRC University, Plot No. IS-2036 to IS-2039 Ramchandrapura Industrial Area, Sitapura, Vidhani, Jaipur, Rajasthan, India-303905, [yogesh.aster@gmail.com](mailto:yogesh.aster@gmail.com)

<sup>2</sup>Department of Mechanical Engineering, JECRC University, Plot No. IS-2036 to IS-2039 Ramchandrapura Industrial Area, Sitapura, Vidhani, Jaipur, Rajasthan, India-303905, [sharmaprofessor18@gmail.com](mailto:sharmaprofessor18@gmail.com)

<sup>3</sup>Department of Mechanical Engineering, JECRC Campus, Shri Ram ki Nangal, via Sitapura RIICO Tonk Road, Jaipur, Rajasthan, India-302 022, [mpsingh.me@jecrc.ac.in](mailto:mpsingh.me@jecrc.ac.in)

\* Corresponding Author

## Abstract:

Welding is a very famous and familiar joining process of similar or dissimilar metals. Welding processes are widely used in industry to manufacture different materials for the use of human beings and their associates. The main objective of this review paper is to study the effect of Tungsten Inert Gas (TIG) welding on Magnesium alloys, Stainless steel, and Aluminum alloys and the impact on mechanical properties and micro-structural control which provides further improvements on alloys. Study shows that in most of the cases tensile strength of weld metal was lower as compared with parent metal in aluminum alloy. The hardness and crystal grains on the fusion zone were very fine and almost the same as a base metal in magnesium alloy. The fatigue life of stainless-steel weld material was observed lower than the base metal. The existence of metal oxides was the core object which influenced the durability of weld.

**Keywords:** TIG welding, mechanical properties, microstructure, Al alloys, Mg alloys, Stainless steel

## 1 Introduction

TIG welding has been broadly active for welding similar and dissimilar materials due to its stability, low cost, and respectable weld quality [1]. Structures used in industries are made up of non-ferrous materials or ferrous materials. The most structural items are oversized extrusion, ingots, and superplastic forming and need machining which creates scrap in large quantities[2]. Tungsten Inert Gas welding is very effective for manufacturing the best quality components, and structures with good industrial capability [3]. During welding, the faying surface of the material is melted and solidified and the weld pool is protected from atmospheric contamination by an inert gas purging out from the TIG torch. Inert gas protects the environmental contamination during welding. The material is melted then solidified and protected by shielding gas [4]. Filler material and groove are required for materials above 2.5 mm thickness with multi passes, fabrication cost, and time [5]. The width of the layer is generally kept in the range of 10–15 mm. The welding layer width is commonly in the choice as 10-14 mm [6-8].

Welding magnesium alloys is a big problem [9]. In the early days, the alloys of magnesium had exciting history and mostly had applications in structures of aircraft manufacturing [10]. By the dominance of deformation mechanisms in twinning and basal slip at atmospheric temperature, the workability of magnesium alloy is poor. Therefore, the elongation to failure of low Mg alloy at an atmospheric temperature generally does not surpass 15% [11]. For welding magnesium alloys gas welding requires careful fluxing to reduce oxidation. The incomplete fluxing and improper cleaning of the weld can cause corrosion in welded structure. Therefore, every magnesium has been welded by applying Tungsten Inert Gas (TIG) technique [9,12]. With proper filler rod metal, the weldability of magnesium alloys is respectable and also minimizes cracking in weld [9]. Aircraft and automotive industries are mostly using aluminum alloy because of its low cost, lightweight, corrosion resistance, and good strength of structure [13-14]. Welding aluminum can be finished by Tungsten

inert gas welding (TIG) with the use of filler material or can be autogenous (without filler material) [15]. Steels are mostly used in automobiles, ships, locomotives, defense, fabrication industries, and many more. Vehicles generally have armor-grade quenched and tempered steels due to hardness, good energy absorption properties, and high strength [16]. The decent performance on corrosion and mechanical properties is found in austenitic steels [17]. TIG welding was achieved by one pass in the bead on a plate on a 9.4 mm thick stainless steel plate. To achieve the increasing demand in production, the deep penetration should increase which rises the life of welded equipment [18-19]. Further, a genetic algorithm was established and this gives solutions in sets [20].

## 2 Outcomes of TIG on Magnesium

Lasahina. T et al did their investigation on a 4 mm thick plate of AZ31 magnesium which was welded by not using any type of filler wire in an AC pulsed TIG welding machine. Observations of microstructure were passed by considering the pulse frequency on the optimum welding conditions and its effect on microstructure. It was detected by using a 20 Hz pulse frequency that the hardness of the fusion region and crystal grains in the fusion area is very fine which is almost equal to the base metal. The joints which are not pulsed had identical elongation and tensile strength as same as a base metal. It was observed that the elongation and tensile strength of 20 Hz pulse welded frequency at joints is high and at base metal, it is lesser but the fatigue limit is 92% at base metal because the fatigue limit of the pulse welded joints is contingent on the grain size of the fusion zone [21].

Liu Liming et al investigated a degreased sample of AZ31B magnesium alloy of 1.7 mm thick plate and used a copper plate of 1 mm thick as the base material for lap joint by TIG welding. Investigation of micrograph was done on electronic microscope JSM 6500LV and tension-shear tests were carried on CSS-2250 electronic tension machine. Results showed a diffusion layer of 150  $\mu\text{m}$  in the interfacial region between magnesium and copper alloy. The iron plate was kept between magnesium alloy and copper to prevent diffusion due to its high melting point but it was difficult to protect the interface between the iron plate and magnesium alloy. Because of heavy oxidization, the tensile strength is lower as compared to the iron plate. [22]

Liu Xu-he et al finished an investigation to find microstructural and mechanical properties of Mg-Li alloy through TIG welding on a super light 2 mm thick plate. The tensile strength of base metal was 160 MPa and elongation was 34.7% before welding. The samples and welding wire were cleaned and the samples were fixed to prevent dislocation. After welding, microstructures were investigated by optical and scanning electron microscopy, and alloying elements' distribution was determined by dispersive X-ray spectroscopy. Macro morphology results showed no crater cracks and weld beadings. The tensile test fracture, on HAZ, showed lower mechanical properties on weld due to coarser grain than on FZ. The bend test showed similar ductility on the front and back, which means no difference in the properties of the welding procedure. The fracture face was dark and rough in HAZ and had a cleavage plane and dimples. The grain boundaries had enriched Al and Ce. [23]

Jun Shen et al did an experiment using TiO<sub>2</sub> coating on AZ31 magnesium alloy joints and found effects of welding current on mechanical properties, macro morphology, and microstructure by TIG welding process. Specimen dimensions were 100 X 50 X 6 mm of hot extruded ZA31 Mg alloy was properly jigged for butt welding tests. Both with or without TiO<sub>2</sub> coating used different welding currents for different samples. With TiO<sub>2</sub>, increased D/W ratio, the larger grain size in a sample at HAZ and FZ with decreased microhardness when temperature increases, deeper weld penetration and increased ultimate tensile strength at the start and decreased as current increases with a coating at 130A welding current. [24]

Tong Wen et al finished work to find the high-frequency vibration influence on mechanical properties and microstructure by tungsten inert gas (TIG) welded joints of AZ31 Mg alloy had 1-3 mm thick sheets with various groove angles. The process used ultrasonic vibrations by the piezoelectric effect which was generally used to conduct various tests under many vibrating conditions such as groove angle, vibration amplitude, and vibration direction. The coarse structure was not observed in the zone near to fusion line as limited HAZ and Al particles in AZ31 alloy were helpful for grain refinement as well as brittle and hard beta phase can let down the toughness and improves the strength. Further, mechanical properties were improved due to horizontal and vertical vibration on all samples but it is lesser in comparison to the parent metal. The vibration was helpful for grain refinement because vibration easily removes the impurities and bubbles from the weld pool. [25]

Bo Qin et al investigated the mechanical properties and microstructure on joints of AZ61 and ZK60 Mg alloy thru TIG and A-TIG welding with dimensions of 80 X 40 X 3 mm. Further samples were cut into dog bone shapes for tensile tests and polished for microstructure analysis. Larger grains size was observed in the HAZ region and refined grains in the FZ region on AZ61 compared to base metal, as well as growth of grains on ZK60, was matched to AZ61. The interaction coefficient of Zn and Mg can be calculated as  $\lambda_{Mg-Al} = -7.272$  kJ/mol. Phase identification on DSC curves presented that the temperature region of molten metal of AZ61 Mg alloy is larger than ZK60 Mg alloy whereas solidus temperature of ZK60 Mg alloy was larger than AZ61 Mg alloy as shown in figure 5. The tensile strength of AZ61 was greater than ZK60 whereas the tensile strength of ZK60 and AZ61 Mg alloy at various currents was greater than TIG welded AZ61/ZK60.[26]

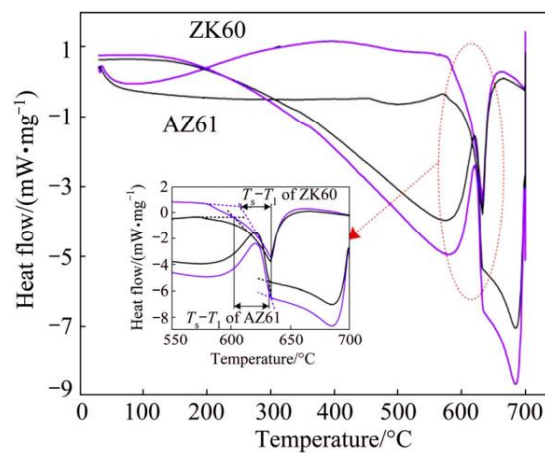


**Fig. 1.** DSC curves of AZ61 and ZK60 magnesium alloys

**Table 1.** TIG welding literature on Mg

S. No.	Author's	TIG Variant	Material	Outcome
1	Xiaodong Qi et al., (2010), [27]	Laser TIG	AZ31B Mg Alloy, 1.7 mm thick	The observation shows that the corrosion may affect the welding joint properties.
2	Abbas Assar et al., (2021), [28]	TIG conventional welding,	AZ91 Mg alloy, 10 mm thick	The tensile strength of the weld specimen was below compared of the parent metal and the heat i/p increased with a decrease in tensile strength.
3	A. Munitz et al., (2001), [29]	AC square-wave penetrating welding	AZ91D Mg, 4 mm thick	The magnesium AZ91D with 4 mm thickness can be effectively TIG welded. No defects were observed in heat affected zone or weld.
4	M. Abbas et al., (2012), [30]	TIG conventional welding,	Mg-alloy	The porosity was improved at 170A and 180A & with an increment in heat i/p values, then the trend of growth of solidification cracking was also augmented.
5	Zhu T et al, (2008),	TIG welding,	AZ91 Mg cast alloy,	The regular change of re-

	[31]	conventional		solidifying microstructure inside partially melted zone from parent metal to welded metal was considered.
6	Carlone P et al., (2015), [32]	TIG welding, conventional	ZE41A Mg alloy	AMS 4439F standard was adopted for welding processes to get satisfactory welding joints. Fine grains were detected in the TIG joints' fusion zone.
7	Braszczyńska-Malik KN et al., (2011), [33]	TIG welding, conventional	AZ91 Mg alloy, 15 mm thick	The welding arc efficiency ranges from 0.63 to 0.88. The increase in welding speed and welding current increases the efficiency of melting.
8	ChenbinLi et al, (2012), [34]	Laser TIG	AZ61 Mg alloy, 2 mm thick	With the increase in speed of welding, the average grain size and linear energy decline on the assertion which completely penetrated on joints had no microscopic cracks or pores.
9	Tong Wen et al., (2015), [35]	Laser TIG	AZ31 Mg alloy, 1-3 mm thick	The microhardness in the fusion zone increases and the average grain size in the fusion zone decreases with an increase in the speed of welding.
10	Paweł Nowak et al., (2016), [36]	TIG welding, conventional	Mg alloys, 20 mm thick	The Mg alloy doesn't weaken the resistance by corrosion through welding. The corrosion resistance is inferior compared to Mg alloy and other alloys.

### 3 The outcome of TIG on Aluminum

Urena. An et al took a sample of aluminum alloy 2014/SiC/XP having X as 6, 13 & 20 %. The fractures that occurred after the test found that the samples had 50% less tensile strength compared with the properties of the parent metal. It was deduced from studies thru transverse preparation (LM & SEM) and fracture (SEM) that the interfacial failure increases in welded material with the development of Al<sub>4</sub>C<sub>3</sub> and this reduces the strength of reinforcement & matrix interface and controlling the size and quantity of cracked particles [37].

R. A. Owen et al did their experiment on AA 2024 using the TIG welding process to measure the synchrotron and neutrons of residual strain present in the aluminum alloy during testing for aerospace structures. Using MIGATRONIC TIG commander 400 AC/DC on 160 mm of length and 150 mm of width specimen, the study was shown to examine the softening and natural aging. Since measurement of strain was done concurrently in two perpendicular directions. Bruker GADDS area detector shows the differences in strain. Results showed that maximum tensile stresses are nearly 60% of the original yield stress. The finite element model technique was possibly the effect on stress of weld considering concurrent different weld procedures and finally,

diffraction tastings and FE analysis gave the idea for validated welding procedures and advancement of robust techniques for aerospace structures [38].

Wang Rui et al experimented with 5A12 aluminum alloy and BT20 titanium alloy of dimensions 200 X 160 X 2.5 mm by overlaying welding tests using TIG welding to study the dynamic process of both metals and used four displacement sensors parallel to weld and one temperature sensor near the weld. Descending longitudinal bending and transverse shrinkage werethe main aspects that induced dynamic angular distortion in the welding process. The distortion of BT20 titanium alloy was bowled at the initial stage and the displacements at the center of the sample were observed larger compared to the edges. The distortion of 5A12 alloy bowled at the initial stage and the displacement at the edges of the sample was observed larger compared to the middle. The change properties of both alloys are different in the thermal cycle and the temperature of BT20 alloy keeps stable after welding but the temperature increases after welding in 5A12 alloy. The equilibrium temperature of the BT20 alloy is lower as compared to the 5A12 alloy and the temperature gradient of the 5A12 alloy is lesser than BT20 alloy, this showed that greater distortion can be produced at high equilibrium temperature [39]

Yang Dongxia et al studied mechanical properties and microstructures by laser beam welding and TIG welding on an AL-Mg-Mn-Er alloy plate of 200 X 100 X 1.7 mm sample. The butt joint was welded using OTC OSACOM SUPER 8700 TIG welder and high-power Nd: YAG laser with 3kW power. The transmission electron microscope and the optical microscope were used for microstructural study and AG-250KNIS tensile testing system for 70 X 1.5 mm sample to study mechanical properties. Results showed that the fusion area of LBW was 75% and 84% narrower than TIG welding. Microstructures observed were coarser in weld metal of TIG and refine in LBW. Compositions of fusion areas showed evaporation in Mg nearly 22%-36% compared to parent metal by both TIG and LBW because of high equilibrium vapor pressure compared to Al. Mg evaporation is less in LBW as compared to TIG. The tensile strength of LBW is 8% superior tothe TIG joint because of fine-grain strengthening [40].

R. Singh et al did research on 6061 AA and studied the effect of strain rate and notch radius on tensile properties and fracture performance with parent metal sample dimension for the tensile test as 75 X 30 X 3.2 mm and TIG welded sample dimensions was 60 X 30 X 3.2 mm with and without notch on 100kN ADMET, USA. Without a notch,the specimen was fractured from base metal and showed that the strength of base metal was weaker than welded region but continuously decreases as the notch radius increased and the strain rate of parent metal was affected large compared with the welded sample. The hardness of the welded area was recorded as a minimum of upto 60% lesser and the maximum reading may increase upto 20% more compared with the base metal. Experimental data were compared with SED and Neuber's methods for maximum stress at the tip of the notch [41].

Qingdong Qin et al worked on TIG welded Al-Mg<sub>2</sub>Si alloy joints for finding various results of mechanical properties and microstructure on a sample size of 80 x 80 x 2 mm. As in figure 6a, the microstructure of 125 A welded joints shown by OM discovered the presence of eutectic Mg<sub>2</sub>Si and white  $\alpha$ -Al on FZ, and the presence of Mg<sub>2</sub>Si in BM is larger than FZ. The share of high angle grain boundaries and low angle grain boundaries in the fusion zone were not equivalent to base metal considering varying misorientation angles. The hardness of FZ was 45% greater than BM whereas elongation and ultimate tensile strength produced by 125 A current were weaker than BM and ultimate tensile strength at 135 A was equal to BM and elongation was a little greater than BM, microstructure image in figure 6. As the number of cycles increased in the thermal shock test, macroscopic structures were not altered significantly as well as cracks were not produced in the weld joint [42].

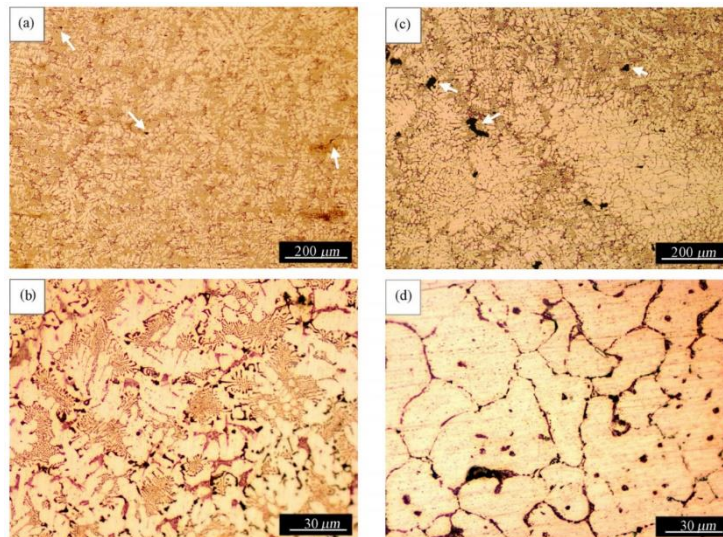


**Fig. 2.** Microstructures of the FZ (a) for a welding current of 125 A and (b) the magnified image of Fig. 6a and those (c) for a welding current of 135 A and (d) the magnified image of Fig. 6c.

D. Nathan et al [43] The welding defects identification and calculations of strength can confirm the dissimilar AA welding usefulness and the workability of dissimilar AA bond was considered through ultrasound test (UT), hardness, LPT, microstructure, visual appearance, and microstructure. The TIG joints of microstructures at various zones were recognized. Similarly, the calculation of hardness values and LPT values was completed. The defects in welding were identified by UT and LPT. Finally, the conclusion is that the joining of dissimilar AA is feasible through TIG welding.

**Table 2.** TIG welding literature on Al

S. No.	Author's	TIG Variant	Material	Outcome
1	Chen et al., (2018), [44]	TIG welding, Conventional	5083 Al plate, 8 mm thick	A 5 lpm boost in GFR increases the weld infiltration depth at the rate of 0.1 mm. The GFR increment from 5 lpm to 20 lpm was observed 30% growth in weld infiltration depth.
2	Kumar Sunderrajan, (2009), [45]	Pulse TIG welding	AA 5456, 2.14 mm thick	Pulse frequency increases with the increase in WAR.
3	V. Mohanavel et al., (2017), [46]	TIG welding, Conventional	AA 6061, 6 mm thick	The most important parameter of welded joints for impact strength is GFR trailed by the speed of welding and lastly welding current.
4	Behnam L et al., (2014), [47]	TIG welding, Conventional	AA 380A, 10 mm thick	The evenly scattering of SiC particles in the dendritic Al matrix is shown in the results.
5	Azwinur et al., (2021), [48]	TIG welding, Conventional	AA 6061, 5 mm thick	At 160A, the lesser hardness value in the HAZ area is 41.17 HRE and the

6	Z.Y. Zhu et al, (2015), [49]	Variable TIG	Polarity AA2219-T87, 8 mm thick	larger hardness value in the area of weld metal is 95.17 HRE. The most critical zone of corrosion observed is HAZ. The vulnerability to the behavior of corrosion for HAZ has been recognized in the segregation and dissolution of grain boundaries along with the Al <sub>2</sub> Cu phase.
7	Kannan et al., (2016), [50]	TIG welding, Conventional	Al 2025 tube, OD 18.8 mm & ID 14.8 mm	The hardness value is 131.364 Hv and the compression strength value is 174.846 MPa was the mechanical properties to attain optimum weld strength.
8	M. Fattahi et al., (2013), [51]	TIG welding, Conventional	1050 AA, 10 mm thick	To upgrade the TIG welded AA and Al mechanical properties, the filler material comprising MWCNT can work as an excellent filler material.
9	G. Sathish Kumar et al, (2022) [52]	TIG Welding	AA6082	The result shows that the hardness and tensile strength decrease as the current increases.
10	Y. Liang et al., (2017), [53]	TIG – CMT hybrid welding	6061 -T6 AA, 4 mm thick	The 40% strength and 50% elongation of the welded joint had been reduced approximately as compared to the parent metal.

#### 4 The outcome of TIG on Steel

Tetsumi Yuri et al investigated to find fatigue properties on base metal and weld metals of SUS304L & SUS316L by considering low and high cycle fatigue properties and the impact of this on weld structure as well as investigation of  $\delta$ -ferrite on fatigue properties at cryogenic temperature to find long life reliability by using liquid hydrogen super tankers and storage tanks to advance a welding process. The S-N curve of both the metals shifted towards the higher or long-life side with frequently decreasing test temperatures. High cycle fatigue strength at weld metals is 0.35-0.7 at 10<sup>6</sup> cycles to tensile strength is falling below compared to the base material with continuously lowering test temperatures. Fatigue crack at SUS304L welded metal had many blowholes of diameter 200-700  $\mu$ m as compared to SUS316L. The low cycle fatigue test shows that the fatigue life of weld material is lower as compared to base metals. In the end, the toughness of  $\delta$ -ferrite is reduced on austenitic SS at cryogenic temperatures as well as high and low cycle fatigue properties are not significant on  $\delta$ -ferrite [54].

G. Lothongkum et al investigated on 3 mm thick AISI 316 L stainless steel plate and used weld bead shapes that resembled DIN 8563 class BS for studied the parameters which had welding speed, % of the time, Pulse/base currents, and pulse frequency. Initial weld results for 6 hrs showed the acceptable weld profile with

complete penetrations as well as 9 hrs test observes the lowest pulse current and it was observed that gravitational force may affect the results. The formation of slag at top of the weld is more as the welding speed is increasing to more than 6 mm/sec and also resulting incomplete filling if the welding speed is above 5 mm/sec.  $\delta$ -ferrite ranges from 6 to 10 % volume in weld range and minimum at 9 hrs. Weld beads shown are free from porosity tested by X-ray test.[55]

S. K. Samanta et al used AISI 316L stainless steel and investigated the effect of rare earth elements on oxidation and microstructure behavior by TIG welding under dry air. Specimen size was 100X50X6 mm and Master TIG MLS 2500 Kemppi was used to weld V shape 90o sample piece. Cerium-doped WMZ of 316L specimen shows vermicular and lacy ferrite nearby fusion boundary and at the center of weld only vermicular ferrite was shown. The availability of Niobium (Nb) with Cerium (Ce) barred the development of chromium carbide and protected the stainless steel from Chromium depletion and gave a result that the presence of Nb and Ce in WMZ showed outstanding resistance property of 316L stainless steel.[56]

Jun Yan et al did an investigation on 304 stainless steel by laser TIG hybrid welding, laser welding, and TIG welding to study the mechanical properties and microstructure of a 3 mm thick 304 SS plate. Porosity and cracks were not found in all types of welding joints. The fusion area and width of the laser joint and the hybrid joint are lesser than the TIG joint. All welding joints were composed of  $\gamma$ -Fe and  $\delta$ -Fe phases.  $\delta$ -Fe content is lower in TIG joints as compared to laser and hybrid joints at a higher cooling rate. Columnar dendrites were observed in laser and hybrid joint and  $\delta$ -Fe as vermicular at transition zone and skeletal at HAZ in TIG joint. Tensile strength was more in the laser joint as compared to the other two joints. Laser and hybrid joints observed dislocation slip due to pure shear while in the TIG joint, necking down region and surface slip were observed. Due to excellent welding speed and mechanical properties, hybrid and laser welding is suitable for 304 SS in industrial applications [57].

Shawan Cui et all investigation was focused on mechanical properties and microstructure evolution of butt welded S32101 duplex stainless steel thru keyhole deep penetration TIG welding by single pass without filler metals and groove penetration on a 10.8 mm thick sample. Penetration was improved with a rise in current and penetration was poor with low welding current. The grains on HAZ become coarser due to welding heat and longer heat shows larger grain growth. Still, successive rapid cooling prevents further grain growth. Temperature gradient at edge and center were relatively large and the high cooling rate of solidification of weld metal. The base metal had uniform misorientation angle distribution of ferrite but misorientation angle distribution of austenite in base metal was observed generally in LAGBs. Misorientation angle distribution of austenite and ferrite in weld metal were observed in LAGBs and grains in weld metal had preferred orientation. Test analyses showed that the toughness of heat affected zone and weld metal was low compared to the base metal. The Microhardness and tensile strength of weld metal were larger than the base metal.[58]

Pramod Kumar et al ANSYS APDL 17.2 software was used for a 3D numerical simulation model to simulate the TIG welding process designed for 320 x 100 x 1.4 mm 304L steel sheet and used to predict the highest temperature, the profile of temperature, and the outcome of varying welding current at constant welding voltage and speed. Observations displayed that as welding current increases, peak temperature also increases at WZ but peak temperature decreases away from WZ at every welding current as well as peak temperature decreases as distance increases from WZ for every case. Figure 7 shows the temperature field distribution at the 49th step at varying welding current and constant welding speed and voltage (a) 25A (b) 75A (c) 115A (d) 145A.[59]

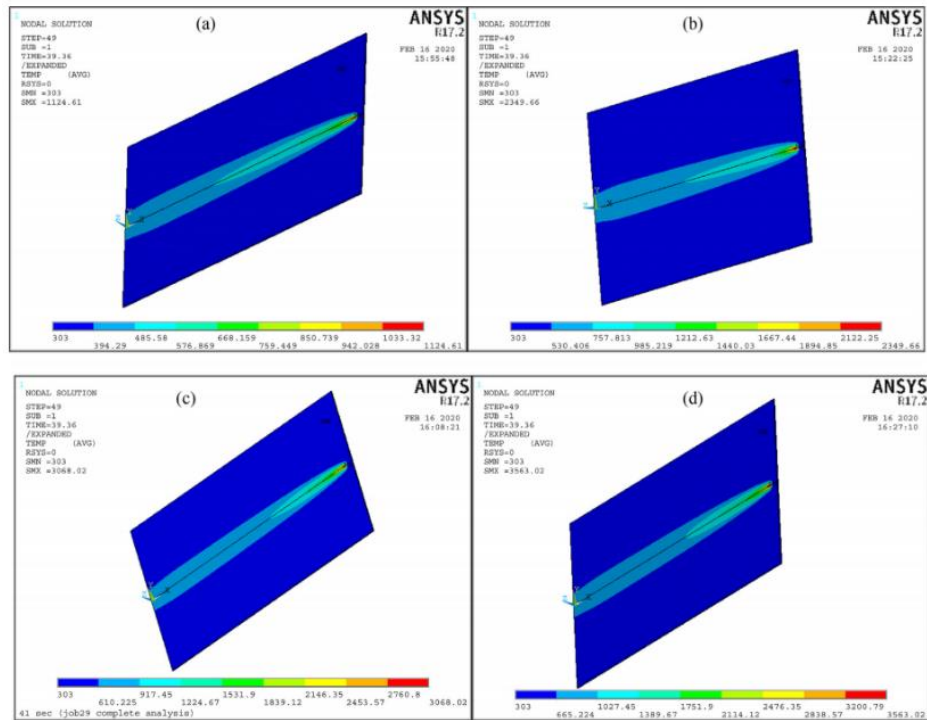


**Fig. 3.** Temperature field distribution at 49th step at varying welding current and constant welding speed and voltage (a) 25A (b) 75A (c) 115A (d) 145A.

**Table 2.** TIG welding literature on Steel

S. No.	Author's	TIG Variant	Material	Outcome
1	Durgutlu et al. (2004), [60]	TIG conventional welding,	316L Austenitic SS, 4 mm thick	All of the chosen pulse GTAW parameters were significant and showed a noticeable influence on clad dilution.
2	S. Bag et al., (2009) [61]	TIG conventional welding,	SS 30436, 3 mm thick	Weld HAZ width, fusion zone (FZ), and depth of penetration increase by an increase in welding current and weld arc energy.
3	Sathiya et al., (2009), [62]	TIG conventional welding,	SS 2205 Alloy, 5 mm thick	Argon shielding gas has a greater weld aspect ratio compared to helium gas in welding bead geometry.
4	Schwedersky et al., (2018), [63]	Multi-tungsten electrode TIG	MS plate (EN 10025-2 S235JR), 10 mm thick	At alike scan speed situation and welding current, the MTE TIG yields serene welding beads while conventional TIG welding yields uneven welding beads. The humping intensity is promoted by lessening the gap between electrodes.

5	Giridharan et al., (2009), [64]	Pulse TIG welding	AISI 304L, 3 mm thick	Increment in welding peak current also advances the weld depth of penetration and width of weld.
6	Sakthivel et al., (2011), [65]	Activated welding	TIG 316L Austenitic SS, 6 mm thick	A-TIG welding technique is enough to yield full penetrated welding joints whereas the conventional TIG technique requires seven or more multiple passes for joining the butt joint.
7	Ramkumar et al., (2015), [66]	Activated welding	TIG AISI 430 steel, 5 mm thick	For AISI 340 steel of 5 mm thick, Fe <sub>2</sub> O <sub>3</sub> needs 140A, and SiO <sub>2</sub> requires 160A to reach complete weld penetration depth. SiO <sub>2</sub> is less effective compared to Fe <sub>2</sub> O <sub>3</sub> .
8	Vasantharaja et al., (2015), [67]	Activated welding	TIG 316LN SS, 10 mm thick	Comparing conventional TIG with A TIG, the A TIG yields 100% growth in welding depth of penetration.
9	Feng et al., (2015), [68]	Keyhole welding	TIG AISI 316L SS, 10 mm thick	At a welding current of 500A at the speed of 310 mm/min, the complete butt welding joint penetration is achievable at a single pass which has been performed through the K-TIG welding technique with the help of filler material and without preparation of edge.
10	Fang et al., (2017), [69]	High-frequency Keyhole TIG	Q345 steel, 5.5 mm thick	To achieve complete penetration on the welding joint at the speed of 390 mm/min, the HFPC at the time of the K-TIG technique can decline the weld current necessity from 430A to 340A.

---

## 5 Conclusion

The Mg is light in weight element as compared to steel, iron alloys, and aluminum for structural and fabrication applications [10]. The welding features are compared between Al & Mg alloys and seen that the surface tension and viscosity of liquid magnesium are below liquid aluminum which can decline the quality of weld surface area and can increase spatters at the process of welding [12].

The tensile strength of the weld joint is less compared to the parent metal of aluminum alloy. The fatigue life of stainless-steel base metal is high compared to the base metal. The crystal grains and hardness of the fusion

zone were fine and almost match with the base metal of magnesium. The weld durability was influenced by metal oxides present in metals.

## References

- 1.Echezona, N.: TIG welding of dissimilar material: A review. *Advances in material science and engineering, LNME*, pp-1-9(2021).
- 2.Singh, S.N. S., Chowdhury, Y.:A Comparative Analysis of Laser Additive Manufacturing of High Layer Thickness Pure Ti and Inconel 718 Alloy Materials Using Finite Element Method Materials.CONFERENCE 2021, vol. 14 (4), pp. 1-18. *Materials today proceeding* (2021).
- 3.Xu, Y.: Computer vision technology for seam tracking in robotic GTAW and GMAW. *Rob. Comput. Integr. Manuf.* 32, 25–36(2015).
- 4.Durgutlu, A.:Experimental investigation of the effect of hydrogen in argon as a shielding gas on TIG welding of austenitic stainless steel. *Mater. Des.* 25, 19-23 (2004).
- 5.Vidhyarthi, R.S.: Activating flux tungsten inert gas welding for enhanced weld penetration. *J. Manuf. Processes* 22, 211–228 (2016).
- 6.Huang, H. Y.: Effects of shielding gas composition and activating flux on GTAW weldments. *Mater. Des.* 30, 2404-9 (2009).
- 7.Mills K.C.: Factors affecting variable weld penetration. *Int. Mater. Rev.* 35, 185–216(1990).
- 8.Huang, H. Y.: Argon–hydrogen shielding gas mixtures for activating flux assisted gas tungsten arc welding. *Metall. Mater. Trans. A. Phys. Metall. Mater. Sci.* 41, 2829–35.
- 9.Liu,L.: Welding materials for magnesium alloys.Welding and Joining of Magnesium Alloys. 1<sup>st</sup> edition.Woodhead Publishing Series in Welding and Other Joining Technologies, (2010).
- 10.Krishnan K. S., Mishrs, R. S.: Chapter-7 Magnesium alloy.Metallurgy and Design of Alloys with Hierarchical Microstructures.345-383 (2017).
- 11.Del Valle, J. A.: Deformation Mechanisms Responsible for the High Ductility in a Mg AZ31 Alloy Analyzed by Electron Backscattered Diffraction, *Metallurgical and Materials Transactions.* vol 36, (2005)1427–1438.
- 12.Polmear,I.,David, S.,Nie, J. F.: 6 – Magnesium alloys, *Light Alloys.* 5<sup>th</sup>edn. *Metallurgy of the Light Metals*, 287-367 (2017).
- 13.Chen, Q.: Grain fragmentation in ultrasonicassisted TIG weld of pure aluminum. *Ultrasonic Sonochemistry* 39 (3), 403–41 (2017).
- 14.Zhang, C.: Relationship between pool characteristic and weld porosity in laser arc hybrid welding of AA6082 aluminum alloy. *Journal of Materials Processing Technology* 240, 217–222 (2017).
- 15.Eisazadeh, H.: Effects of gravity on mechanical properties of GTA welded joints. *Journal of Materials Processing Technology* 214(5), 1136-1142 (2014).
- 16.Zhenyu, F.: Improving the weld microstructure and material properties of K-TIG welded armour steel joint using filler material. *The International Journal of Advanced Manufacturing Technology* (2018).
- 17.Rao, V.: Experimental Investigation for Welding Aspects of Stainless Steel 310 for the Process of TIG Welding, *Procedia Engineering* 97, 902-908 (2014).
- 18.Suman, S.:Productivity improvementin butt joining of thick stainlesssteel plates through the usage of activated TIG welding *SN Applied Sciences* 3, 416 (2021).
- 19.Hidetoshi, F.: Development of an advanced A-TIG (AA-TIG) welding method by control of Marangoni convection. *Materials Science and Engineering A* 495, 296–303 (2008).
- 20.Chandrasekhar, N.: Optimization of hybrid laser–TIG welding of 316LN stainless steel using genetic algorithm. *Materials and Manufacturing Processes* 32(10), 1094–1100 (2017).
- 21.Em,S.:Integr. Clim. Prot. Cult. Herit. Asp. Policy Dev. Plans. *Free Hanseatic City Hambg* 2(4),1–37 (1995).
- 22.Liming,L.: Study on the dissimilar magnesium alloy and copper lap joint by TIG welding. *Mater. Sci. Eng. A* 47(6)(1–2), 206–209 (2008),

- 23.Liu,H. S.: Microstructure and mechanical properties of Mg-Li alloy after TIG welding. *Trans. Nonferrous Met. Soc.* 21(3), 477–481 (2011).
- 24.Shen, J.: Effects of welding current on properties of A-TIG welded AZ31 magnesium alloy joints with TiO<sub>2</sub> coating. *Oral Oncol.* 50(10), 2507–2515 (2014).
- 25.Wen, T.: Influence of high frequency vibration on microstructure and mechanical properties of TIG welding joints of AZ31 magnesium alloy. *Trans. Nonferrous Met. Soc.* 25(2), 397–404 (2015).
- 26.Qin, B.: Microstructure and mechanical properties of TIG/A-TIG welded AZ61/ZK60 magnesium alloy joints. *Trans. Nonferrous Met. Soc.* 29(9), 1864–1872 (2019).
- 27.Xiaodong, Qi.: Interfacial structure of the joints between magnesium alloy and mild steel with nickel as interlayer by hybrid laser-TIG welding. *Materials and Design* 31, 605-609 (2010).
- 28.Assar, A.:Effect of heat input of TIG repair welding on microstructure and mechanical properties of cast AZ91 magnesium alloy. *Welding in the World* 65, 1131-1143 (2021).
- 29.Munitz, A.: Mechanical properties and microstructure of gas tungsten arc welded magnesium AZ91D plates. *Materials Science and Engineering A302*, 68-73 (2001).
- 30.Abbas, M.: Effect of Weld Current and Weld Speed on the Microstructure and Tensile Properties of Magnesium Alloy Specimens during Tungsten Inert Gas Welding. *Technical Journal*19(II), 35-390 (2014).
- 31.Zhu, T.: Microstructure formation in partially melted zone during gas tungsten arc welding of AZ91 Mg cast alloy. *Mater. Charact.* 59, 1550–1558 (2008).
- 32.Carlone, P.: Characterization of TIG and FSW weldings in cast ZE41A magnesium alloy. *J Mater Process Technol* 215, 87–94 (2015).
- 33.Braszczyńska, M. K. N.:Mroz M, Gas-tungsten arc welding of AZ91 magnesium alloy. *J Alloys Compd.* 509, 9951–9958 (2011).
- 34.Chenbin, Li.: Effect of Welding Speed in High Speed Laser-TIG Welding of Magnesium Alloy. *Materials and Manufacturing Processes* 27, 1424–1428 (2012).
- 35.Wen, Tong.: Influence of high frequency vibration on microstructure and mechanical properties of TIG welding joints of AZ31 magnesium alloy. *Trans. Nonferrous Met. Soc.*25, 397–404 (2015).
- 36.Qin, Bo.: Microstructure and mechanical properties of TIG/A-TIG welded AZ61/ZK60 magnesium alloy joints. *Trans. Nonferrous Met. Soc.* 29, 1864–1872 (2019).
- 37.Urena, A.: Influence of interface reactions on fracture mechanisms in TIG arc-welded aluminium matrix composites. *Composites Science and Technology* 60, 613-622 (2000).
- 38.Owen, R. A.: Neutron and synchrotron measurements of residual strain in TIG welded aluminium alloy 2024. *Materials Science and Engineering A346*, 159-167 (2003).
- 39.Wang, R.: Dynamic process of angular distortion between aluminum and titanium alloys with TIG welding. *Trans Non-Ferrous. Met. Soc.* 18, 233-239 (2008).
- 40.Yang, D.: Study on microstructure and mechanical properties of Al-Mg-Mn-Er alloy joints welded by TIG and laser beam. *Mater. Des.* 9(40), 117–123 (2012).
- 41.Singh, R.: Influence of notch radius and strain rate on the mechanical properties and fracture behavior of TIG-welded 6061 aluminum alloy. *Arch. Civ. Mech. Eng.* 16(3), 513–523 (2012).
- 42.Qin, Q.: Microstructures and mechanical properties of TIG welded Al-Mg<sub>2</sub>Si alloy joints. *J. Manuf. Process.* 56, 941–949 (2020).
- 43.Nathan, D.,Ashwin K. S.: Feasibility study of TIG welding of AA6063-AA7075 alloys. In: Vijayan,S., Subramanian,N. (eds.) *TRENDS IN MANUFACTURING AND ENGINEERING MANAGEMENT 2019, LNME*, 709-719. Springer, Berlin (2021)
- 44.Chen, C.: Effects of helium gas flow rate on arc shape, molten pool behavior and penetration in aluminum alloy DCEN TIG welding. *Mater. Process. Tech.* 255(2), 696–702 (2018).

45. Kumar, A.: Optimization of pulsed TIG welding process parameters on mechanical properties of AA 5456 Aluminum alloy weldments. *Mater. Des.* 30 (4), 1288–1297 (2009).
46. Mohanavel, V.: Optimization of tungsten inert gas welding parameters to attain maximum impact strength in AA6061 alloy joints using Taguchi Technique. In: *INTERNATIONAL CONFERENCE ON ADVANCES IN MATERIALS AND MANUFACTURING APPLICATIONS 2017*, Proceedings, vol. 5, pp. 25112–25120. Materials Today, Bangalore (2018).
47. Apolina A. R.: TIG welding with single-component fluxes. *J. Mater. Process. Tech.* 99, 260–265 (2000).
48. Azwinur, S.: Effect of variation of TIG welding current on tensile strength and hardness of aluminium A-6061. *J. of Wel. Tech.* 3(1), 17-22 (2021).
49. Zhu, Z.Y.: Effect of post weld heat treatment on the microstructure and corrosion behavior of AA2219 aluminum alloy joints welded by variable polarity tungsten inert gas welding. *Trans. Nonferrous Met. Soc.* 24(5), 1307 –1316 (2014).
50. Kannan, S.: An investigation on compression strength analysis of commercial aluminium tube to aluminium 2025 tube plate by using TIG welding process. *J. of Alloys and Compounds* S0925-8388(16)30096-2 (2016).
51. Fattahi, M. N.: A new technique for the strengthening of aluminum tungsten inert gas weld metals: Using carbon nanotube/aluminum composite as a filler metal. *Micron* S0968-4328(13)00106-6 (2013).
52. Kumar, G. S.: Investigation of the TIG Welding Process for Joining AA6082 Alloy Using Grey Relational Analysis. *Advances in Materials Science and Engineering*, Article ID 5670172, 8 pages (2022).
53. Liang, Y.: Effect of TIG current on microstructural and mechanical properties of 6061 -T6 aluminium alloy joints by TIG – CMT hybrid welding. *J. Mater. Process. Technol.* 255, 161 –174 (2018).
54. Yuri, T.: Effect of welding structure and  $\delta$ -ferrite on fatigue properties for TIG welded austenitic stainless steels at cryogenic temperatures. *Cryogenics* 40, 251-259 (2000).
55. Lothongkum, G.: Study on the effects of pulsed TIG welding parameters on delta-ferrite content, shape factor and bead quality in orbital welding of AISI 316L stainless steel plate. *J of Mat. Pro. Tech.* 110, 233-238 (2001).
56. Samanta, S. K.: Effect of rare earth elements on microstructure and oxidation behavior in TIG weldments of AISI 316L stainless steel. *Mater. Sci. Eng.* A430 1(2), 242–247 (2006).
57. Yan, J.: Study on microstructure and mechanical properties of 304 stainless steel joints by TIG, laser and laser-TIG hybrid welding. *Opt. Lasers Eng.* 48(4), 512–517 (2010).
58. Cui, S.: Microstructure evolution and mechanical properties of keyhole deep penetration TIG welds of S32101 duplex stainless steel. *Mater. Sci. Eng.* A709, 214–222 (2018).
59. Kumar, P.: Investigation of numerical modelling of TIG welding of austenitic stainless steel (304L). *Mat. Today Pro.* 27(2), 1636–1640 (2020).
60. Durgutlu, A.: Experimental investigation of the effect of hydrogen in argon as a shielding gas on TIG welding of austenitic stainless steel. *Materials and Design* 25, 19–23 (2004).
61. Bag, S.: Development of efficient numerical heat transfer model coupled with genetic algorithm-based optimization for prediction of process variables in GTA spot welding. *Sci. Technol. Weld. Joining* 14(4), 333–345 (2009).
62. Sathiya, P.: Effect of shielding gases on mechanical and metallurgical properties of duplex stainless-steel welds. *J. Mater. Sci.* 44, 114–121 (2009).
63. Schwedersky, M.B.: Arc characteristic evaluation of the double-electrode GTAW process using high current values. *Int. J. Adv. Manuf. Technol.* 98, 929–936 (2018).
64. Giridharan, P. K.: Optimization of pulsed GTA welding process parameters for the welding of AISI 304L stainless steel sheets. *Int. J. Adv. Manuf. Technol.* 40(5–6), 478–489 (2009).
65. Sakthivel, T.: Comparison of creep rupture behaviour of type 316L(N) austenitic stainless steel joints welded by TIG and activated TIG welding processes, *Mater. Sci. Eng.* A528, 6971–6980 (2011).

66. Ramkumar, K. D.: Comparative studies on the weldability, microstructure and tensile properties of autogeneous TIG welded AISI 430 ferritic stainless steel with and without flux. *J. Manuf. Processes* 20, 54–69 (2015).
67. Vasantharaja, P.: Effect of welding processes on the residual stress and distortion in type 316LN stainless steel weld joints. *J. Manuf. Processes* 19, 187–193 (2015).
68. Feng, Y.: Keyhole gas tungsten arc welding of AISI 316L stainless steel. *Mater. Des.* 85 24–31 (2015).
69. Fang, Y. X.: Improving Q345 weld microstructure and mechanical properties with high frequency current arc in keyhole mode TIG welding. *Journal of Materials Processing Technology* S0924-0136(17)30326-6.